Crystalline microstructure and mechanical properties of crosslinked EPDM aged under gamma irradiation

Emilie Planès, Laurent Chazeau, J.-M. Chenal, Gérard Vigier, Thomas Stuhldreier

Crystalline Microstructure and Mechanical Properties of Crosslinked EPDM Aged Under Gamma Irradiation

EMILIE PLANES,[1,2] LAURENT CHAZEAU,[1] GÉRARD VIGIER,[1] JEAN-MARC CHENAL,[1] THOMAS STUHLDREIER[2]

[1]Uníversité de Lyon, INSA-Lyon, MATEIS CNRS UMRSS10, Bâtiment Blaise Pascal, 20 Avenue Albert Einstein, F-69621 Villeurbanne, Cedex, France

[2]Nexans Research Center, 170 Avenue Jean Jaurès, F-69353 Lyon Cedex 07, France

ABSTRACT: The morphology and the mechanical properties at room temperature of crosslinked EPDM irradiated or not have been studied. It has been shown that these materials are composed of two phases: semicrystalline zones with a crystallinity ratio of 20% and mainly amorphous zones. The semicrystalline zones make a continuous path through the film and therefore control the mechanical properties of the material below the melting temperature. As irradiation (in the tested range of irradiation dose) and crosslinking degree have no significant influence on the arrangement and proportion of the crystalline lamellae, all samples have nearly the same mechanical behavior at small strains. At large strains, the interactions between amorphous and crystalline parts in semicrystalline zones play the main role in the mechanical response; irradiation, by degradation of these interactions, leads to a smaller hardening phenomenon and a decrease in elongation at break. From an application point of view, in spite of the low crystallinity fraction of these materials, the presence of an important number of crystallites, as evidenced by SAXS measurements, strongly limits the consequences of irradiation on the mechanical properties. However, the mechanical reinforcement strongly depending on the presence of these crystallites, it is therefore highly sensitive to temperature: this can be an important issue for the applications of these materials since their use temperature is close to the crystallite melting temperature.

KEYWORDS: ageing; crystallization; structure-properties relations

INTRODUCTION Polymers are in some cases used in environments where they may be exposed to high-energy radiation, for instance, in nuclear power plants. Over the years, the effects of high-energy radiation on polyethylene have been extensively studied.[1–5] Irradiation causes the material aging: indeed, important changes such as crosslinking and chain scissions often occur simultaneously. Many factors such as the polyethylene (PE) type, the absorbed dose, and irradiation conditions—temperature, dose rate, and the irradiation atmosphere—largely influence these processes. Given the semicrystalline nature of polyethylene, the influence of the crystalline morphology on the irradiation mechanism and its evolution during this irradiation are issues to also consider. Although crystallites can also be sensitive to gamma irradiation, the polymer parts mainly affected by the degradation are in the amorphous state, because of the weak permeability of oxygen in crystallites.[3] Thus, the crystalline part of the material essentially influences the degradation intensity by reducing the polymer fraction concerned by the degradation mechanism, i.e., the amorphous one. Nevertheless, Bateja[2] has reported that with an increasing radiation dose (at relatively small doses) in the open air, the degree of crystallinity of polyethylene increases. Indeed, chain scissions in the amorphous regions can create small chains which can crystallize at temperature lower than the crystallization temperature of the unaged polymer. Therefore, the crystalline part, if not involved in the degradation mechanisms, seems to be involved in the structural evolution of the material during/after degradation.

Ethylene-Propylene-Diene Monomer elastomer (EPDM) is usually preferred to PE for cable application. Like PE, it is a semicrystalline polymer, the crystallinity level of which depends on its content of ethylene monomer entities. An usual ethylene content of 70% leads to a crystallinity level of around 10%.[6] This is much less than common linear polyethylene in which the crystallites represent the major part of the material. This means a material more sensitive to irradiation.[7] Indeed, as the crystallite thickness is very small, this leads to melting temperature which can be relatively low and closer to the room temperature, and therefore to the temperature at which irradiation is usually performed. Such crystalline morphology is of main importance in the mechanical properties of the polymer. Indeed, Celette et al.[5] have

Correspondence to: L. Chazeau (E-mail: laurent.chazeau@insa-lyon.fr)

shown that the semi crystalline nature of EPDM at room temperature strongly attenuates the effect of degradation. Despite a large degradation of the polymer evidenced above the melting temperature, they found only small difference in properties when measured at room temperature. This suggested few modifications of the crystalline phase during irradiation. However, it was not demonstrated by a microstructural characterization of the material.

Thus, the aim of this work is to relate the microstructural modifications induced by irradiation to the mechanical properties of the material, those including the stiffness and the ultimate properties. The degradation mechanisms of the studied materials have been presented in a previous paper[7]: EPDM elastomers have been aged by gamma irradiation at room temperature under oxygen atmosphere and their mechanical properties have been studied at 80 °C. Except a crosslinking process in its early stage of degradation, this degradation mainly consists of chain scission whose the consequences are a decrease in the modulus and more generally in the material stiffness, and a degradation of the ultimate properties. Moreover, the rupture behavior can be related to the initial crosslink density (as far as the degradation mechanism has not totally destroyed all the shortest chains) and the sol fraction, this one including at high irradiation doses, portion of active chains and free agglomerates of initially active chains. Thus, this article completes such results by a study of the mechanical properties and microstructure of the material at room temperature, i.e., below the melting temperature, as a function of the irradiation dose.

EXPERIMENTAL

Materials

The studied EPDM elastomer is a statistic copolymer and is composed of 70% ethylene, 29.5% propylene and 0.5% ethylenedienenorbornene (ENB). An analysis by size exclusion chromatography (SEC) gave the following results: M_w 39,300 g/mol, M_n 5140 g/mol and $I_p = 7.65$. The samples are processed as follows. The polymer matrix and the crosslinking agent are mixed in the internal mixer (5 min of pre-mixing of the matrix followed by the addition of 3 phr of dicumyl peroxide (Perkadox BC-FF from Akzo Nobel) and mixing for 10 min at low temperature, 80 °C). A second mixing is performed in an external mixer (cylinders) for 10 min at 80 °C. Then the compound is pressed as 1-mm-thick films at 170 °C during 10 min to promote crosslinking reaction. The curing time is determined from torque measurement performed with a MOSANTO analyzer. It is evaluated as the time needed to reach 98% of the maximum torque extrapolated at infinite curing time. Two types of EPDM materials have been processed: uncrosslinked and crosslinled ones. They will be called hereafter E-NC and E-CR materials respectively. An EPDM elastomer has also been processed with a smaller curing time, 2 min, to obtain a material with a lower crosslinking degree. It will be called hereafter E-CR2min.

Irradiation Conditions

E-CR samples are exposed to γ-radiation of a ^{60}Co source at a dose rate of 1 kGy/h in an oxygen atmosphere for doses 50, 165, 300, 510 kGy (Arc Nucleart—Grenoble France): the water temperature of the pool, where exposures are performed, is around 18 °C. Afterwards, the samples are stored under vacuum at about 22 °C. The samples will be named hereafter E-CR-XXX with XXX the irradiation dose.

Characterization Techniques

Tensile Tests

Tensile tests are performed with an MTS 1/ME device equipped with a temperature controlled chamber. An image processing acquisition system (Apollor VideoTraction System) is used to obtain true stress-true strain curves. Experiments are conducted at 25 °C with a true strain rate 0.01 s^{-1}. Three specimens are tested for each material. The samples are dumbbell-shaped with gauge dimensions $20 \times 4 \times 1$ mm^3. On figures only one test is reported, but another figure with the average stresses and strains at break of the three specimens and error bars is also presented.

The elastic modulus E at 25 °C and at 80 °C is calculated as the slope at the origin of the true strain-true stress curve.

Differential Scanning Calorimetry

All measurements are made with a Perkin—Elmer Diamond calorimeter, with 7—8 mg of material encapsulated in standard aluminum pans. Dry nitrogen is used as the purge gas. The instrument is calibrated with indium using a scan rate corresponding to the heating rate of the experiments.

The crystallization temperature domain of our EPDM is large:[6] from about −40 °C up to 60 °C. Indeed, when the polymer is cooled from 80 °C to −50 °C, one wide peak can be observed during the heating ramp, as shown in Figure 1(a). If an isothermal treatment of several hours at the temperature T_c is performed during cooling, three melting peaks are obtained during the heating scan [cf. Fig. 1(b)]:

- One, which corresponds to the crystallite population formed during cooling from 80 °C to T_c.
- A second one, which concerns the crystallite population formed during the isothermal treatment at T_c.
- And a third one, which corresponds to the crystallite population, created during the cooling from T_c to −40 °C.

Test series have been performed to evaluate the optimal crystallization temperature, i.e., the temperature T_c which leads to the highest crystallinity ratio with the fastest crystallization kinetic. The optimized isothermal treatment for 12 h at 22 °C enabled generating stable crystallinity.

Thus, the thermal treatment applied to all samples is the following [cf. Fig. 1(c)]:

- A heating ramp up to 80 °C to erase the thermal history.
- A rapid cooling down at 50 °C/min to the optimal crystallization temperature 22 °C and storage during 12 h at this temperature.

Moreover, in order not to affect the crystallinity by any further treatments around this temperature, in particular

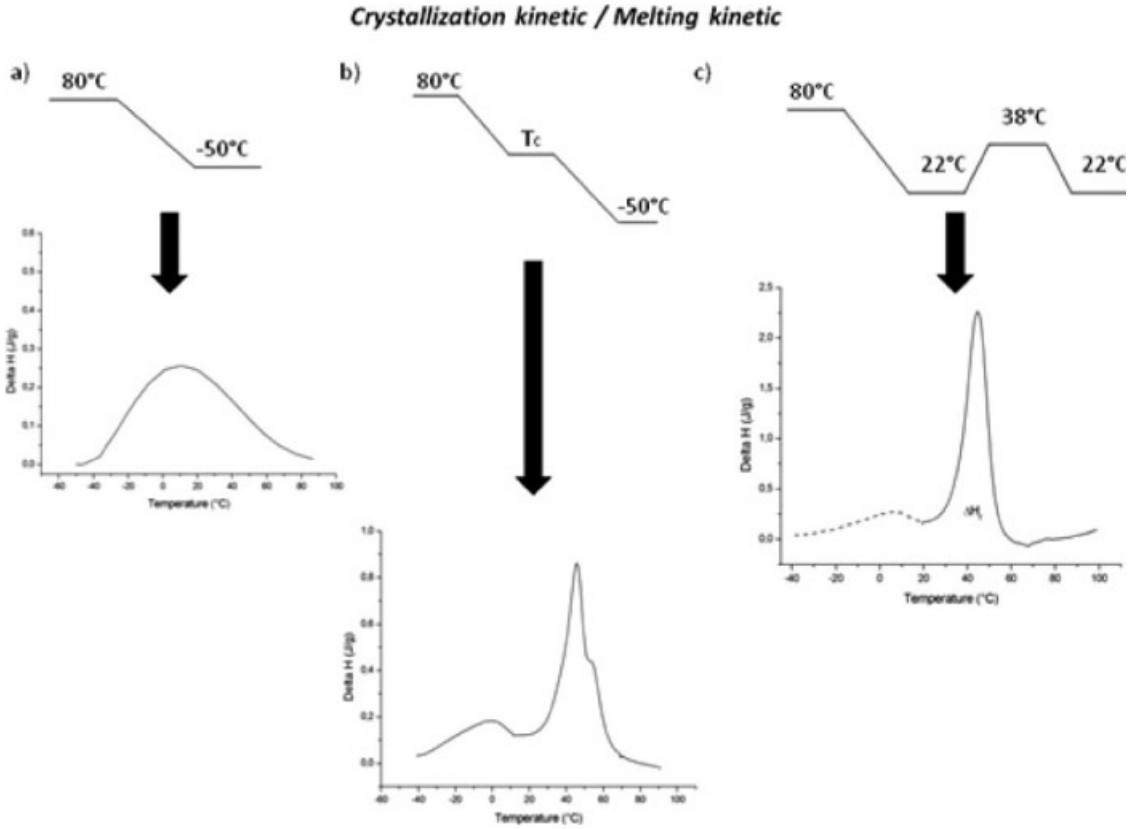

FIGURE 1 Crystallization and melting DSC curves of EPDM.

during the aging in the irradiation pool at 18 °C, and the storage at 22 °C after irradiation, the samples are annealed by a heating ramp at 1 °C/min up to 38 °C and maintained at this temperature during 6 h. Then they are cooled down to 22 °C and stored at this same temperature. This treatment enables to get a crystallite population with a well defined peak with a melting temperature above 22 °C.

To study the materials crystallinity after their irradiation, samples are cooled from room temperature down to −50 °C at the cooling rate of 10 °C/min and heated up to 100 °C at 10 °C/min. The cooling from room temperature to −50 °C is necessary to avoid the overlap of the DSC starting overshoot with the melting peaks. But this cooling induces supplementary crystallization and the formation of an additional melting peak, which can be observed between −40 °C and 20 °C. Therefore, the weight crystallinity ratio X_{cw} is defined from enthalpy of the melting peaks between 22 °C and 60 °C ΔH_f.

$$X_{cw} = \frac{\Delta H_f}{\Delta H_{f0}} \tag{1}$$

ΔH_{f0} is taken equal to 290 J/g,[8] which is the value for perfect polyethylene crystal, since it is assumed that only polyethylene segments can crystallize. This weight crystallinity ratio can be converted in volume crystallinity ratio X_{cv} using the density value of the crystalline polyethylene (1.006 g/cm^3[38]) and of the amorphous part of this copolymer. The latter is estimated from the amorphous polyethylene (0.855 g/cm^3) and amorphous polypropylene (0.854 g/cm^3) densities[8] and is taken equal to 0.855 g/cm^3.

SAXS Measurements

Small-Angle X-ray Scattering (SAXS) are carried out on a device equipped with a copper rotating anode (λ = 1.54 Å) with Gobel's mirror point collimation system and 2D detector (Princeton Instrument SCX2D). The scattering vector domain is deduced from the detector-sample distance. The scattering vector is directly correlated to the scattering angle 2θ and the wavelength λ:

$$q = (4\pi/\lambda)\sin\theta \tag{2}$$

In our experiments, the detector-sample distance is fixed at 1160 mm and the corresponding q domain is: 0.01−0.08 nm^{-1}. The patterns are acquired during 5 min for SAXS measurements and they are corrected from background scattering and thickness.

From SAXS patterns (cf. Fig. 2), the long period L_{PB} characteristic of the regular stacking of crystal blocks and amorphous layers can be evaluated. Using Bragg's law and the position of the maximum q_{max}, L_{PB} is calculated following:

$$L_{PB} = \frac{2\pi}{q_{max}} \tag{3}$$

L_{PB} represents the sum of the average thickness of the crystal lamellae l_c, and of the interlamellar amorphous areas l_a. This method does not directly provide any values for l_a or l_c.

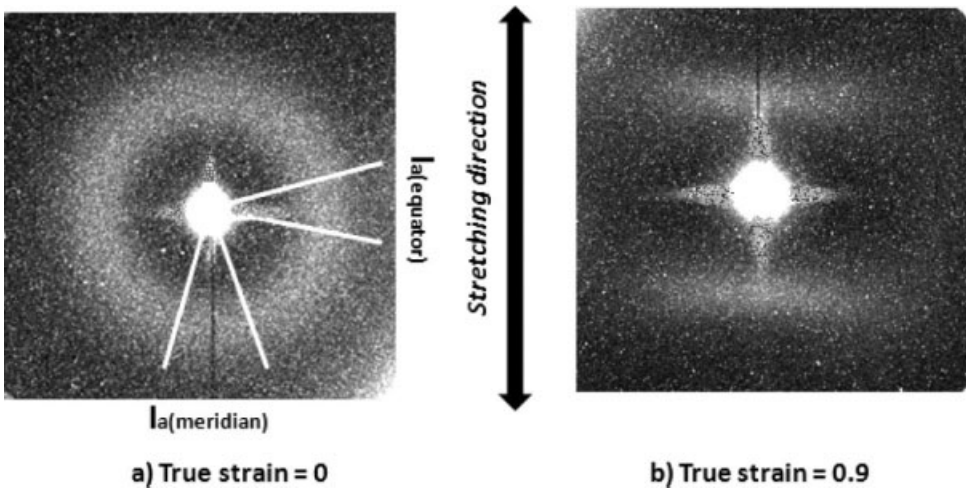

FIGURE 2 SAXS patterns of E-CR-0 during stretching: (a) unstretched (b) at 0.9 true strain.

The correlation function is used in order to obtain the structural parameters: l_a, l_c. Linear correlation function is calculated by a cosine transformation of the intensity curves $I(q)$.[9,10]

$$\gamma(r) = \frac{\int_0^\infty I(q)q^2 \cos(qr)dq}{\int_0^\infty I(q)q^2 dq} \quad (4)$$

where r represents the distance in real space. In practice, data are not recorded from zero to infinity but over a restricted q-range. Therefore, the procedure of integration to infinity involves the use of a polynomial extrapolation in the scattering region of the beamstop, i.e., at low scattering angle, such as:

$$I(q) = Aq^\alpha \quad (5)$$

And at large scattering angles, the data are extrapolated with the Porod's law:

$$I(q) = \frac{B}{q^2} + \frac{C}{q^4} \quad (6)$$

Where B depends on the deviation from the Porod's law and tends towards 0 for a neat interface (no roughness, sharp electron density gradient...) and C is the Porod constant.[11] From the correlation function, in addition to the L_{PB} values obtained from Lorentz corrected SAXS profile, another estimation of this parameter, called hereafter L_{PC}, can be performed from the position of the first maximum of the correlation function. Moreover a volume crystallinity ratio can be obtained from this curve.

In Situ *SAXS Measurements During Stretching*

A homemade stretching machine allowing the symmetric deformation of the sample was used to probe by X-ray the same sample area during stretching at 0.04 min^{-1} strain rate and at room temperature. The two-dimensional (2D) SAXS patterns were recorded every 5min. The long periods in the stretching direction and perpendicular to the stretching direction were computed by a radial integration of the 2D SAXS patterns over sectors of $\pm 20^\circ$ around the meridian and the equator, i.e., the directions parallel and normal to the tensile axis (cf. Fig. 2).

RESULTS AND DISCUSSIONS

Microstructure of Unaged Sample and Undeformed Sample

The crystalline phase of E-CR is characterized by DSC. The curves are presented in Figure 3. The melting peak located at 45 °C is very large. This indicates crystals with a large thickness distribution that would be due to the broad sequence distribution of ethylene moiety along the polymer chain. Moreover, the position of the melting peak is similar for E-CR and E-CR2min. The melting peak of E-NC is larger

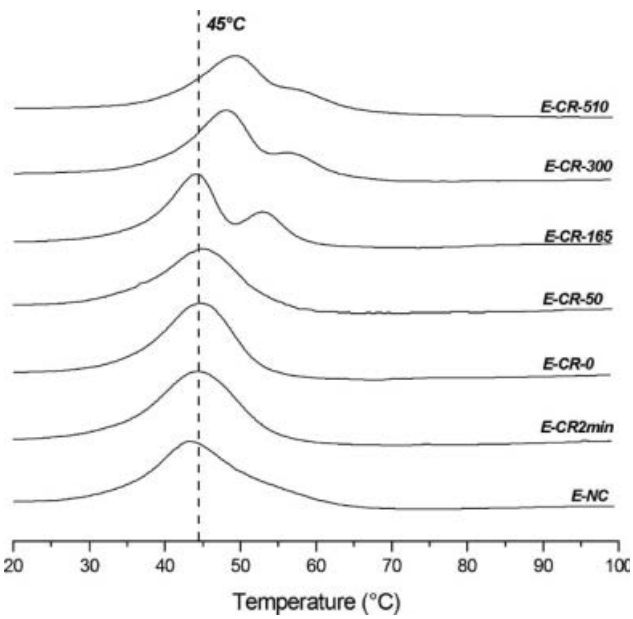

FIGURE 3 DSC analyses for the studied materials.

TABLE 1 Results Deduced from DSC Analyses and SAXS Experiments

Sample Name	X_{cw} (%) ±0.2	X_{cv} (%) ±0.2	T_{f1}/T_{f2} (°C)	X_{ci} (%)	L_{PB} (nm)	L_{PC} (nm)	l_c (nm)	l_a (nm)	σ (J/m^2)
E-CR-0	10.6	9.1	45	25	12.9	10.8	2.7	8.1	0.09
E-CR-50	10.3	8.9	45	24	13	11.2	2.7	8.5	0.09
E-CR-165	10.4	9	44/53	23	12.5	11.5	2.7	8.8	0.09
E-CR-300	11.9	10.3	48/57	21	14.2	13.5	2.9	10.6	0.09
E-CR-510	10.9	9.4	50/59	22	13.2	11.7	2.6	9.1	0.08
E-CR2min	11.4	9.8	45	21	13.5	12	2.7	9.3	0.09
E-NC	12.4	10.7	43	23	14.2	13	2.7	10.3	0.09

and depressed by 2 °C with regard to the others materials. Given the measurements uncertainties of 0.2%, the weak difference of crystallinity ratio found for the different materials are significant. The volume crystallinity data reported in Table 1 are 9.1%, 9.8%, and 10.7% for E-CR, E-CR2min, and E-NC respectively. These ratios are correlated to the crosslink density of materials: the less crosslinked the rubber, the higher the crystallinity. This was expected since it is known that crosslinks hinder the crystallization growth.[12] Following the literature,[13,14] this crystallinity ratio should correspond to a fringed micelles morphology. To have more insights on the morphology, SAXS experiments have been performed.

The SAXS pattern of E-CR in the undeformed state (cf. Fig. 2) shows an isotropic scattering ring which indicates a periodic structure. Thus, this SAXS peak can be attributed to alternating crystalline and amorphous lamellae. This means that the microstructure is more organized than that suggested by the works of Bensason et al. and Minick et al.[13,14] However, the correlation peak is not pronounced, which indicates that it is a structure with an important disorder. In addition, the crystallite organization of this type of copolymer was also evidenced in a paper of Liu et al.[6] and will be confirmed by the *in situ* SAXS experiments during stretching presented later. Given these results, we think reasonable to consider the structure as lamellar for further data analysis.

The long periods deduced from Bragg's law and from the correlation function (L_{PB} and $L_{PC,}$ respectively) are reported in Table 1. Both methods give similar results and the values are nearly independent on the crosslink density of E-NC (L_{PB} equals to 13.5 ± 1 nm). l_c values, determined from the correlation curves, are reported in the same table and they are also similar for the three EPDM materials. These values (2.7 nm) are much lower than those obtained for a medium or low density polyethylene (PE) (around 10−20 nm[15,16]). This explains the low melting temperature. From the Gibbs-Thomson relation, the surface energy can be deduced:

$$\sigma = \Delta H_f^0 \rho l_c \frac{T_f^0 - T_f}{2T_f^0} \tag{7}$$

where T_f^0 is the melting temperature of an infinite crystal, ΔH_f^0 is the melting enthalpy per unit mass of an infinite crystal, ρ is the crystalline density and l_c is the thickness of the crystals. In the case of PE, $T_f^0 = 140$ °C, ΔH_f^0 to 290 J/g and $\rho = 1.006$ g/cm^3 at room temperature. Taking the same data for the three EPDM materials of the study, the found σ value for the three EPDM materials is 0.09 J/m^2 (cf. Table 2). It is closed to the value found by Kazmierczak et al.[17] for PE (0.09 J/m^2) or by Darras et al.[15] for ethylene-butene random copolymers (0.06−0.1 J/m^2). This σ value suggests that the microstructure is similar to that of PE. Moreover, some microstructural information can be extracted from the calculation of the crystallinity ratio. The crystallinity ratio can be deduced from SAXS by two methods. The first one, X_{ci} is directly deduced from the l_c/L_{PC} ratio, since we assume here a lamellar structure:

$$X_{ci}\ (\%) = \frac{l_c}{L_{PC}} \times 100 \tag{8}$$

Within the same assumption, a second crystallinity ratio X_{cc} can be deduced from the minimum value of the correlation function following[9]:

$$X_{cc} = \frac{\gamma_{min}}{\gamma_{min} - 1} \tag{9}$$

The first methods gives values around 23% (±2%), while the second method gives slightly inferior values of 17%, whatever the EPDM materials. X_{cc} determined from γ_{min} underestimates generally the true value of the crystallinity. Thus the two methods give very similar results. These values are much higher than the X_{cv} values deduced from DSC analyses (around 10%). This promotes the idea of the existence of two phases: one rich in crystalline lamellae called hereafter "semicrystalline zone" and another one very poor in crystalline lamellae called hereafter "amorphous zone." We can estimate the volume fraction of the semicrystalline zone Φ_{sc}, assuming that the crystallinity ratio of the semicrystalline zone is given by X_{ci} or X_{cc}, i.e., is about 20% and roughly zero for the amorphous zone:

$$\phi_{sc}\ (\%) = \frac{X_{cv}}{X_{ci}} \times 100 \tag{10}$$

Whatever the uncertainties on the chosen X_{ci} values, ϕ_{sc} is around 50%. With the values of Table 1, 43%, 57%, and

TABLE 2 Soluble Fraction, Swelling Ratio, Elastic Moduli of the Different Materials

Sample Name	Soluble Fraction* (%)	Swelling Ratio*	Elastic Modulus at 80 °C (MPa)	Elastic Modulus at 25 °C (MPa)
E-NC	100	–	–	8.2 ± 0.8
E-CR2min	0 ± 3	5.7 ± 0.6	1.5 ± 0.2	7.8 ± 0.8
E-CR-0	0 ± 3	3.7 ± 0.4	2.9 ± 0.3	5.8 ± 0.6
E-CR-50	2.9 ± 3	3.7 ± 0.4	3.1 ± 0.3	5.8 ± 0.6
E-CR-165	5.7 ± 3	4.1 ± 0.4	2.6 ± 0.3	5.8 ± 0.6
E-CR-300	8.8 ± 3	4.8 ± 0.5	2.1 ± 0.2	6 ± 0.6
E-CR-510	20.6 ± 3	6.2 ± 0.6	1.2 ± 0.1	5.9 ± 0.6

* These experimental data are borrowed from the paper of Planes et al.[7]

65% are found for E-CR, E-CR2min and E-NC respectively, i.e., a value which increases when the crosslink density decreases. It is impossible from SAXS measurements to characterize the distribution of these zones in the material. However, the elastic modulus provides some insights on this distribution.

Table 2 gives the modulus values at 80 °C and at 25 °C for the three EPDM materials. The elastic modulus at 80 °C is directly related to the crosslink degree of the amorphous phase; it is not measurable for E-NC. At 25 °C the reinforcement provided by the crystallites is evidenced, in particular for uncrosslinked EPDM. Despite the low crystallinity ratio, the small size of the crystallites suggests that they are numerous. Consequently, they can be assimilated to crosslinking nodes, which play a predominant role in the mechanical properties. Moreover, the modulus is correlated to the crystallinity ratio X_{cv} (cf. Fig. 4).

It is noteworthy that at this temperature E-NC shows the highest modulus. If the semicrystalline zones were not continuous in this material, the elastic modulus at 25 °C value would be very low (especially if one considers the low molecular weight of the studied EPDM). Therefore the semicrystalline zones make a continuous path. All ϕ_{sc} and X_c values being in the same range for the three EPDM materials, it is reasonable to consider that this is true for all of them. The parallel and series models can be studied. The series model does not work since the E-NC material has a much higher modulus than the amorphous phase. The parallel model, which assumes that the amorphous zones are mechanically parallel to the semicrystalline ones, gives:

$$E = \phi_{sc} \times E_c + (1 - \phi_{SC}) \times E_a \qquad (11)$$

Where E_c is the elastic modulus of semicrystalline zone and E_a is the modulus of the amorphous zone. Taking for Φ_{sc} 0.65 and for E the experimental value of 8.2, and considering E_a as negligible, the deduced value for E_c is 13 MPa. This is between two and three times lower than the value found in our laboratory for a PE with a crystallinity ratio X_{ci} equals to 20%.[18] This suggests that the mechanical behavior of the studied materials should be described by a combination of series and parallel models. This will be confirmed by *in situ* SAXS experiments during tensile tests presented in "Tensile Tests" section. In addition, considering Brown's approach[19] for computing of tie chain probability, the very low crystal thickness in the material should result in a high density of tie chains in comparison with medium or high density PE. Moreover, as reported in literature, conversely to ethyl or butyl branches, the inclusion of the methyl branches of the propylene units in the crystallites is possible under near-to-equilibrium conditions,[20,21] but such inclusions are defects and therefore less likely. This might lead to a slight enrichment in PE of the amorphous part in the semicrystalline zones and, given the statistical nature of the copolymer, this might also lead to more numerous tie molecules.

Microstructure Evolution During Stretching of Unaged Samples

Figures 5 and 6 present the true strain–true stress curves at room temperature; Figure 2(b) presents the corresponding SAXS patterns of E-CR measured *in situ*. The behavior

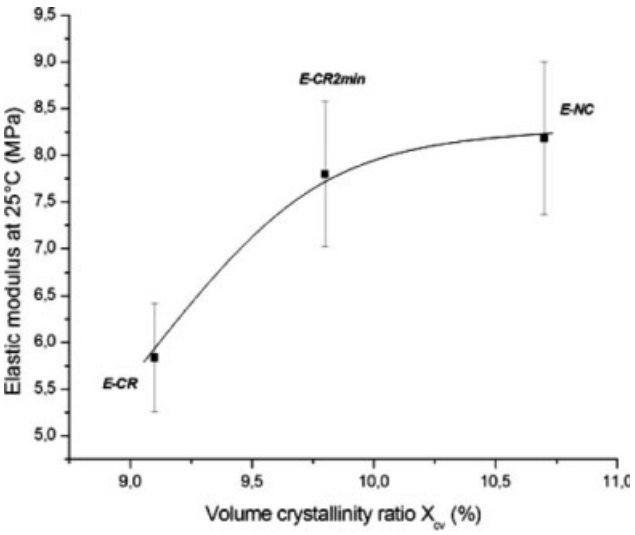

FIGURE 4 Evolution of the elastic modulus at 25 °C with the crystallinity ratio X_c for E-CR, E-CR2min, and E-NC (the dashed line is a guideline for the eyes).

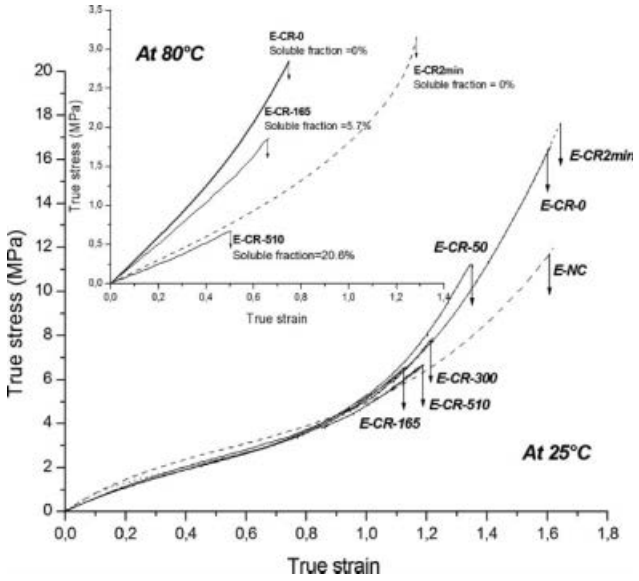

FIGURE 5 Large strain behavior at 25 °C and at 80 °C (in insert) of studied materials.

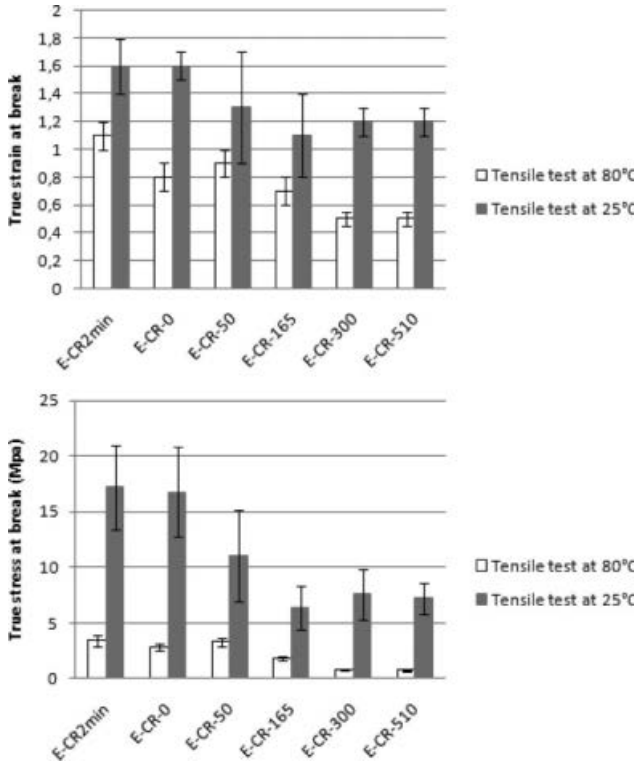

FIGURE 6 Average strains and stresses at break of three specimens tested with error bars for tensile tests at 80 °C and at 25 °C.

observed in SAXS is similar to that of PE: the pattern ovalization is followed by the appearance of two maxima occurring perpendicular to the stretching direction. The Figure 7 (L_{PB} as a function of true strain) illustrates the evolution of L_{PB} (deduced from Bragg's law) in the stretching direction and perpendicular to this direction during the uniaxial deformation. The calculated results for E-CR-0 show that L_{PB} in the stretching direction increases from 13 nm to 15 nm (i.e., about 15% changes) at a 0.3 true strain. At the same strain, perpendicularly to the stretching direction L_{PB} decreases of about 10%. Thus, the semicrystalline phase is deformed, but at a level lower than the macroscopic deformation. Therefore, the mechanical behavior of this "two phases" material should be described by a series/parallel model, as discussed in previous section. The tensile deformation enlarges the average spacing between the crystalline lamellae, which are oriented perpendicularly to the stretching direction (by stretching of the amorphous phase between crystalline lamellae), while it decreases the average spacing between the lamellae oriented parallel to the stretching direction. The magnitude of this phenomenon is larger than that usually observed on polyethylene. This is due to the large amount of amorphous phase in the semicrystalline zone. Between 0.3 and 0.6 true strain, the structure turns into a fibrillar structure (Fig. 7). Conversely to PE, no necking is observed during this transition. This can be explained by two facts: (i) the temperature of the α_c relaxation occurring in the crystalline phase[22,23] which controls the crystalline shearing should be much lower than for classical PE. In the case of PE, this temperature is around 50 °C at 1Hz. The α_c relaxation is directly related to the crystalline lamella thickness. From the results of Popli et al.[22] and from the l_c values previously deduced from SAXS (2.7 nm), it can be estimated that the α_c temperature of our copolymer is lower than room temperature. Roughly speaking it means that the stretching of our samples at room temperature is equivalent to stretching PE samples closed to their melting temperature (around 100 °C). (ii) The large number of tie molecules leads to a very homogeneous distribution of the stress along the crystalline lamellae and prevents strain localization.

The strains at break at room temperature are larger than at 80 °C (see Figs. 5 and 6). Indeed the crack propagation is

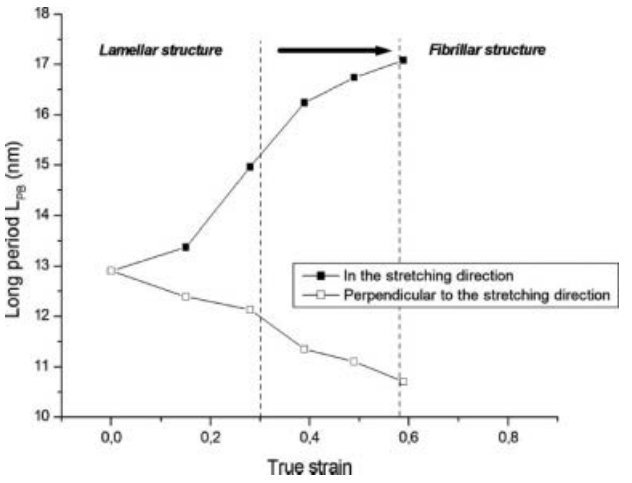

FIGURE 7 Evolution of the long period L_{PB} in the stretching direction and perpendicular to the stretching direction during stretching for E-CR-0.

more difficult in fibrillar structure than in a wholly amorphous material. Conversely to what is observed at 80 °C, the E-NC stress-strain curve at 25 °C shows a hardening, but this hardening is still lower than the one observed for E-CR (Fig. 5). According to the theory of rubber elasticity, the presence of this hardening at room temperature for the uncrosslinked EPDM can be explained by the presence of crystallites, which act as crosslinking nodes. However, the difference in hardening between E-NC and E-CR materials is small which indicates that the chemical crosslinking of the amorphous phase is not the main responsible of the observed hardening.

Consequences of Gamma Irradiation

E-CR has been submitted to different irradiation doses as explained in the experimental section. The irradiated samples have been characterized by DSC. The thermograms presented in Figure 3 show the appearance of a new melting peak at 54 °C for 165 kGy, which vanishes for the highest irradiation dose. Moreover, above 165 kGy dose, an increase in the temperatures of the two melting peaks can be observed.

This can be the signature of either the formation of a second crystallite population and the growth of both crystallite populations (as evidenced by the increase in their melting temperature) or to a process of melting-recrystallization-melting[24,25] occurring during the DSC heating ramp. Nevertheless these two melting peaks correspond to two crystallite populations with very similar thicknesses: from Gibbs-Thomson equation, taking the same value for surface energy σ (0.09 J/m^2), we find 2.7 and 2.9 nm for the melting temperatures of 45 °C and 55 °C, respectively. Thus DSC is very sensitive to any change of lamella thicknesses especially in the case of very small thicknesses. Therefore, it can be concluded that the microstructure evolution during irradiation is very small, in spite of the small changes observed in DSC. This is confirmed by SAXS experiment, since l_c and L_{PC} (or L_{PB}) are found quasi-constant whatever the irradiation dose (cf. Table 1). The crystallinity ratio X_{cv} is almost constant with a slight maximum, around 12%, for 300 kGy dose (cf. Table 1). This is probably due to a slight chemically induced crystallization process up to 300 kGy assisted by chain scissions, which promotes the growth of crystallites. Indeed, chain scissions can increase the polymer mobility in the crystallite vicinity and therefore promote their growth by short chain addition. Note that these phenomena have been also reported in the case of polyethylene materials where they are found to be more important,[2,3] probably because of an initially higher crystallinity ratio. At elevated irradiation dose (510 kGy), X_{cv} begins to decrease: it could be explained by an eventual beginning of the crystallites degradation.[3] Nevertheless, it can still be concluded that irradiation does not induce important modification of the crystallinity ratio and of the proportion of semicrystalline and amorphous zones. Conversely, the amorphous parts of these zones are highly affected as evidenced by the evolutions of the sol fraction and of the swelling ratio with an increasing irradiation dose (cf. Table 2).

The Figure 8 presents the evolution of the elastic modulus at 25 °C with an increasing irradiation dose. For comparison, the moduli at 80 °C are reported on the same figure. The evolution of elastic modulus at 25 °C with the irradiation dose is very limited (5.9 ± 0.2 MPa), especially when compared to that obtained at 80 °C, when the modulus decreases of a factor around 2.5. This decrease, as well as the presence of an increasing sol fraction with irradiation dose, is related to the degradation of the polymer network (cf. Table 1). Thus, in spite of the small crystalline content, the crystallites strongly limit the irradiation consequences on the modulus variation at 25 °C. Note that a slight maximum can be noticed for the 300 kGy dose, in agreement with the variation of crystallinity ratio; though such comment must be considered with caution since the discussed variation are small.

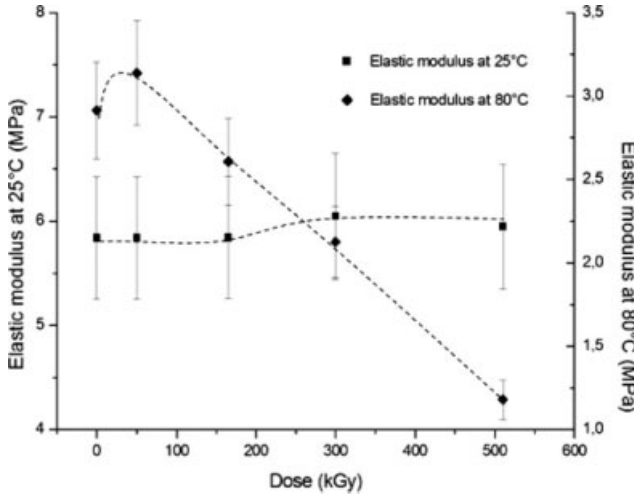

FIGURE 8 Evolution of the elastic modulus at 25 °C and at 80 °C with an increasing irradiation dose (The lines are guides for the eyes.).

Figure 5 gives the true stress−true strain curves of the different samples at 25 °C. Up to a true strain of 1, all curves are nearly superimposed. Conversely, the rupture behavior of the material seems largely influenced by the irradiation dose. Irradiation leads to a large decrease in the elongation and stress at break. Given the uncertainties of the measurement, samples irradiated at 165 kGy, 300 kGy, and 510 kGy give about the same strain and stress at break, the 50 kGy sample giving intermediate values. Hardening seems also to decrease with the irradiation dose; however this phenomenon can also be partly masked by the early rupture of the samples. At true strain <1, one can consider that the mechanical behavior is controlled by the crystallite spatial organization, this one being very similar whatever the irradiation dose or even whatever the crosslinking degree. At larger strains, the fibrillar structure and the interconnecting regions between the fibrils depend on the tie molecules, the crosslinking degree, and the entanglement density. These parameters strongly evolve during irradiation. This is evidenced by the behavior at 80 °C recalled in insert of Figure 5. Especially, it is well known that a decrease in tie molecule concentration, induces a weaker hardening and a more brittle behavior of semicrystalline polymers.[26,27] The most irradiated sample (510 kGy) has a modulus at 80 °C

comparable to that of E-CR2min, i.e., an average crosslink density comparable to that of the E-CR2min. Nevertheless at 25 °C the strain at break of E-CR-510 is lower than the one of E-CR2min (cf. Figure 5). Two explanations can be given: (i) the properties of the amorphous zones are very different: indeed at 80 °C the strain at break of E-CR2min is 2.5 higher than for E-CR-510; therefore the microcracks of the amorphous zones could pilot the rupture of the material at 25 °C; (ii) the irradiation has induced a decrease in tie molecules concentrations in the semicrystalline zone; this phenomenon can be enhanced by their chemical nature: the presence of propylene sequences in the chain provoke their ejection out of the crystallite and can promote the formation of tie molecules. These propylene sequences are likely more sensitive to irradiation: their scission is favored compared to that of ethylene.

If now we compare E-CR2min and E-CR-0, the rupture behavior is nearly the same at 25 °C while it is very different at 80 °C. The amorphous zones present at 25 °C should have the same mechanical properties than the amorphous phase at 80 °C. Thus this result suggests that the rupture behavior at 25 °C is actually not governed by the amorphous zones properties but by the semicrystalline zones and the concentration of tie molecules. As these two materials have similar crystallinity ratios, it seems that the key parameter of rupture behavior is the concentration of tie molecules.

CONCLUSIONS

The morphology and the mechanical properties of EPDM irradiated or not, have been studied. It has been shown that these materials are composed of two phases: semicrystalline zones with a crystallinity ratio of 20% and mainly amorphous zones. The semicrystalline zones make a continuous path through the film and therefore control the mechanical properties of the material in its semicrystalline state for small deformations. At true strain < 1, the spatial organization and the proportion of crystallites control the mechanical properties. As irradiation (in the tested range of irradiation dose) and crosslinking degree have only a small influence on these arrangements and proportions, all samples have nearly the same mechanical behavior. At large strains, the interactions between amorphous and crystalline parts in semicrystalline zones through tie molecules seem to play the main role in the mechanical response. The concentration in tie molecules decreases with an increasing irradiation dose, which explains a smaller hardening phenomenon and a decrease in elongation at break. From an application point of view, it is shown that despite the low crystallinity fraction of these materials, the presence of a large number of crystallites strongly limits the consequences of irradiation on the mechanical properties when the materials are tested in the semicrystalline state. However the mechanical reinforcement mainly depending on these crystallites, it is therefore very sensitive to temperature: this can be an important issue for applications such as cables for nuclear power plants, since their use temperature is close to the crystallite melting temperature.

The authors acknowledge the joint research program "COPOLA" between EDF, NEXANS France, LABORELEC, CEA, INRA and CNRS, for its financial support. The authors also thank J.C. MAJESTE for GPC analyses.

REFERENCES AND NOTES

1 Charlesby, A.; Von Arnim, E.; Callaghan, L. Int J Appl Radiat Isot 1958, 3, 226−231.

2 Bateja, S. K. J App Polym Sci 1983, 28, 861−872.

3 Aslanian, V. M.; Vardanian, V. I.; Avertisian, M. H.; Felekian, S. S.; Ayvasian, S. R. Polymer 1987, 28, 755−757.

4 Geetha, R.; Torikaia, A.; Yoshidad, S.; Nagayab, S.; Shirakawa, H.; Fueki, K. Polym Degrad Stab 1988, 23, 91−98.

5 Celette, N.; Stevenson, I.; Davenas, J.; David, L.; Vigier, G. Nucl Instrum Methods Phys Res B 2001, 185, 305−310.

6 Liu, L. Z.; Hsiao, B. S.; Ren, S.; Fu, B. X.; Toki, S.; Zuo, F.; Tsou, B.; Chu, B. Polymer 2006, 47, 2884−2893.

7 Planes, E.; Chazeau, L.; Vigier, G.; Fournier, J. Polymer 2009, 50, 4028−4038.

8 Polymer Handbook; Bandrup, J.; Immergut, E.; Grulke, E., Ed; Wiley: New York, 1999.

9 Glatter, O.; Kratky, O., Eds.; Small Angle X-Ray Scattering; Academic Press: London, 1982.

10 Goderis, B.; Reynaers, H.; Koch, M. H. J.; Mathot, V. B. F. J Polym Sci Part B: Polym Phys 1999, 37, 1715−1738.

11 Koberstein, J. T.; Morra, B.; Stein, R. S. J Appl Cryst 1980, 13, 34−45.

12 Chenal, J. M.; Chazeau, L.; Bomal, Y.; Gauthier, C. J Polym Sci Part B: Polym Phys 2007, 45, 955−962.

13 Bensason, S.; Minick, J.; Moet, A.; Chum, S.; Hiltner, A.; Baer, E. J Polym Sci Part B: Polym Phys 1996, 34, 1301−1315.

14 Minick, J.; Moet, A.; Hiltner, A.; Baer, E.; Chum, P. J Polym Sci Part B: Polym Phys 1995, 58, 1371−1384.

15 Darras, O.; Seguela, R. Polymer 1993, 34, 2946−2950.

16 Humbert, S.; Lame, O.; Vigier, G. Polymer 2003, 50, 3755−3761.

17 Kazmierczak, T.; Galeski, A.; Argon, A. S. Polymer 2005, 46, 8926−8936.

18 Humbert, S.; Lame, O.; Vigier, G.; Segueto, R. Submitted to Polymer.

19 Brown, Y.-L.; Huang, N. J Polym Sci Part B: Polym Phys 1991, 29, 129−137.

20 Wunderlich, B. Macromolecular Physics. Academic Press: New York, 1976; Vol. 1, Chapter 2.4.

21 Oleinick, E. F. Polym Sci Ser C 2003, 45, 2139−2264.

22 Popli, R.; Glotin, M.; Mandelkern, L. J Polym Sci Part B: Polym Phys Ed 1984, 22, 407−448.

23 Nitta, K. H.; Asuka, K.; Liu, B.; Terano, M. Polymer 2001, 42, 1219−1226.

24 Groenickx, G.; Reynaers, H.; Bergmans, H.; Smets, G. J Polym Sci Part B: Polym Phys Ed 1980, 18, 1311−1324.

25 Vandermiers, C.; Moulin, J. F.; Damman, P.; Dosiere, M. Polymer 2000, 41, 2915−2923.

26 Seguela, R. J Polym Sci Part B: Polym Phys 2005, 43, 1729−1748.

27 Cazenave, J.; Seguela, R.; Sixou, B.; Germain, Y. Polymer 2006, 47, 3904−3914.